Adsorption of Thiol-Protected Gold Nanoparticles on TiO_2 and Their Behavior under UV Light Irradiation

Igor Dolamic, Cyrille Gautier, Julien Boudon, Natallia Shalkevich, and Thomas Bürgi*

Université de Neuchâtel, Institut de Microtechnique, Laboratoire de chimie physique des surfaces, Rue Emile-Argand 11, 2009 Neuchâtel, Switzerland

Received: December 4, 2007; In Final Form: February 7, 2008

A combination of in situ attenuated total reflection infrared (ATR-IR) spectroscopy, UV−vis spectroscopy and transmission electron microscopy was used to study the adsorption of thiol-protected gold nanoparticles on TiO_2 films and the behavior of the resulting composite films upon UV irradiation. The gold nanoparticles were covered by charged thiols *N*-acetyl-L-cysteine and L-glutathione and had a mean core diameter of about 1 nm. The TiO_2 film was prepared by deposition of a slurry of TiO_2 nanoparticles with a particles size of 21 nm. The combination of the two spectroscopic techniques showed that the adsorption of the gold nanoparticles onto the TiO_2 films is significantly limited by intrafilm diffusion. Upon illumination the IR spectra revealed the removal of the adsorbed thiolates and the appearance of sulfates. These species were also observed when *N*-acetyl-L-cysteine adsorbed on TiO_2 was illuminated, i.e., in the absence of gold. In the latter case oxalate was observed in large quantity on the TiO_2 surface, in contrast to the illumination of the *N*-acetyl-L-cysteine-protected gold particles. This indicates a different pathway for the decomposition of the adsorbed thiol when adsorbed on the gold or directly on the TiO_2 surface. In situ UV−vis spectroscopy also shows the formation of larger particles upon illumination, which is confirmed by transmission electron microscopy.

Introduction

Materials composed of gold nanoparticles and a semiconducting support such as TiO_2 are considered for various applications for example in surface patterning,[1] catalysis,[2−4] photocatalysis[5] and photovoltaic cells.[6] In the latter case the excitation of the semiconductor−metal nanocomposite by (sun)light induces electron-transfer processes that may be used for solar energy conversion,[7] i.e., for the production of hydrogen by water splitting. Activity and selectivity of such materials and catalysts strongly depend on the size of the gold particles.[8]

Different methods were considered in the past to prepare Au−TiO_2 catalyst materials such as metal ion impregnation and deposition-precipitation followed by drying, calcination and reduction.[9] During such procedures the Au particles or clusters are formed directly on the support. However, these methods have some disadvantages. The uneven precursor-solution loading due to gravitational forces leads to polydispersity of the resulting metal particles. The necessary thermal treatment furthermore results in severe agglomeration problems and may even cause chemical modification of the support through ionic diffusion.[5] Therefore, alternative methods for catalyst preparation are highly desirable. A different route relates to the preparation of metallic Au^0 particles in solution and subsequent deposition on the TiO_2.[5] This allows better control of size and size distribution of the particles. Very small particles can be prepared by methods that are based on passivating ligands such as phosphines[10] and thiols.[11] These ligands prevent the particles from agglomeration in solution. Once the gold particles are deposited on the TiO_2, the passivating ligands can be removed by calcination of the material. It was for example shown that calcination at 300 °C leads to the removal of thiols as evidenced by X-ray photoelectron spectroscopy (XPS).[4] Calcination was also shown to lead to a moderate increase in the average particles size from 3.4 to 4.6 nm. The resulting material was active in the epoxidation of propylene.

Not only was the release of thiolates from gold surfaces achieved by thermally breaking the S−Au bond, but also reductive desorption of sulfur[12] and thiolate oxidation by I_2[13] and reactive oxygen species[14] was shown. It was furthermore reported that photogenerated radicals can efficiently liberate alkanethiolate ligands in a solution of monolayer-protected gold nanoparticles.[15] The exposure of alkanethiolate self-assembled monolayers (SAM) on gold surfaces to UV light (254 nm) leads to the oxidation of the thiolate to the sulfonate,[16] which can be used to pattern SAMs. Similarly, oxidized sulfur species were reported after exposing a film of thiol-stabilized gold nanoparticles to UV light. Such treatment leads to the coagulation of the gold particles, which enabled the convenient fabrication of gold structures on surfaces.[1] Thiolate removal from gold particles under UV irradiation was assigned to plasmon photoelectrochemistry, i.e., to charge separation and redox reactions.[17] Furthermore, TiO_2 itself is a photocatalyst, which can be used to mineralize organic compounds.[18]

The removal of thiolates from gold surfaces and nanoparticles by light is an important process for the preparation of tailored catalyst materials and for the fabrication of patterned surfaces. However, the occurring processes are not very well understood due to the lack of direct molecular level information from the respective interfaces during irradiation, which hinders the more rational design of (catalyst) materials. Here we use in situ UV−vis and attenuated total reflection infrared (ATR-IR)[19,20] spectroscopy to study the adsorption of charged gold nanoparticles from aqueous solution on TiO_2 particle films and the processes occurring during subsequent irradiation.

* Corresponding author. Tel: ++41 32 718 24 12. Fax: ++41 32 718 25 11. E-mail: thomas.burgi@unine.ch.

10.1021/jp711442m CCC: $40.75
Published on Web 03/26/2008

SCHEME 1: Structure of *N*-Acetyl-L-cysteine and L-Glutathione

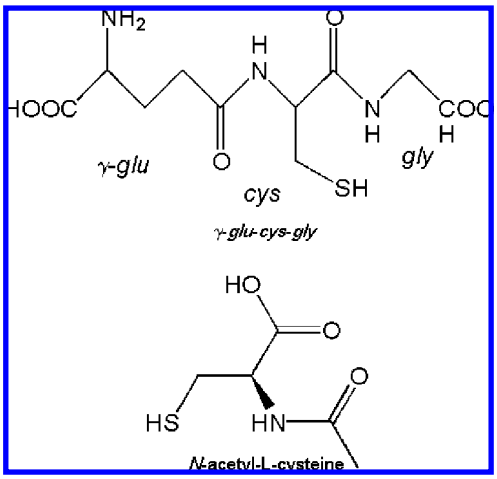

Experimental Section

Materials. Degussa P25 TiO_2 with a surface area of 51 m^2 g^{-1}, average primary particle size of 21 nm and a tapped density of approximately 130 g/L was used. The preparation of the gold particles of about 1 nm core size used in this study was described in detail in previous reports.[21,22] Briefly, 1.01 mmol (400 mg) of tetrachloroauric acid and 4.06 mmol *N*-acetyl-L-cysteine (glutathione) were dissolved in 200 mL of 6:1 methanol:acetic acid, giving a red solution, which rapidly turned into a cloudy white suspension. After 15 min a freshly prepared aqueous $NaBH_4$ solution (70 mL, 2.13 mol/L) was slowly added under vigorous stirring. After 90 min of additional stirring, the resulting solution was filtered using 0.2 μm PTFE membranes (Millipore) to remove precipitates and subsequently evaporated under vacuum to near dryness. The nanoparticles were purified in two steps. The first one consisted of a series of precipitations with ethanol and filtration using 0.2 μm PTFE membranes. The removal of the remaining unreacted thiol or disulfide was finally completed by dialysis (Spectra/Por CE, molecular weight cutoff MWCO = 3500). Particles were dissolved in 30 mL of water and loaded into a membrane, which was then placed in a 2 L beaker of water and slowly stirred. The water was changed every 10 h over the course of 96 h. The black solution was evaporated under vacuum at $T \leq 40$ °C to give a black powder.

HCl (0.1 M, Carlo Erba) was used to adjust the pH. *N*-Acetyl-L-cysteine (NAC, Scheme 1, Sigma-Aldrich >99%) and glutathione (GSH, Scheme 1, Sigma-Aldrich >99%) were used as received. All other reagents were analytical grade and used as received. Milli-Q water (18 MΩ cm) was used in all experiments.

Thin Film Preparation. A slurry was prepared from about 20 mg of P25 TiO_2 and 25 mL of water. After sonication (Ultrasonic cleaner, Branson 200) for 30 min, TiO_2 thin films were formed by dropping the slurry onto a Ge internal reflection element (IRE, 52 mm × 20 mm × 1 mm; KOMLAS). The amount of slurry for one coating was typically about 0.5 mL. The solvent was allowed to evaporate, and the procedure was repeated several times, which allows one to adjust the film thickness. After drying for several minutes at 40 °C in air, loose catalyst particles were removed by flowing water over the IRE. After drying in the air, the film was ready for use. From the amount of deposited TiO_2 and its density an average film thickness was estimated. Films of about 4 μm and 70 μm thickness were prepared. Note that for dense TiO_2 films prepared by a sol−gel method UV light has a penetration depth of a few micrometers.[23] However, light incident on a powder can penetrate substantially deeper than that by diffuse reflection. Direct evidence that the UV light penetrates the TiO_2 films as used here stems from initial experiments with ZnSe internal reflection elements. We have noticed that the UV lamp induces a chemical reaction on the surface of the ZnSe, which results in a color change from yellow to orange. (That is why Ge elements were used in this work.) This color change was also observed with the TiO_2 film present, which shows that the UV light reaches the IRE surface through the TiO_2 film.

Methods. In situ ATR-IR spectra were recorded with two different flow-through cells. The first one was used for combined ATR-IR and UV−vis spectroscopy.[24] The second one was used for ATR-IR spectroscopy during UV irradiation.[25] The latter cell was made from a Teflon piece, a fused silica plate (45 × 35 × 3 mm) with holes for inlet and outlet (36 mm apart), and a flat (1 mm) Viton seal. The cell has a volume of 500 μL. The cell for combined ATR-IR and UV−vis spectroscopy was made of Teflon with a volume of 77 μL and a gap between IRE and the surface of the cell of 250 μm. The ATR cell is equipped with a fused silica window (5 mm diameter and 3 mm thickness), which allows simultaneous recording of UV−vis and ATR-IR spectra. The distance between the inlet and outlet of the ATR cell is 36 mm, and the window for UV−vis spectroscopy is positioned 10 mm from the outlet. A UV−vis probe was positioned in front of the window perpendicular to the IRE surface, such that the end of the probe was located approximately 4 mm above the catalyst layer. The probe (AVANTES) consists of six fibers that guide the light from a deuterium halogen source to the sample and one fiber that guides the reflected light to a UV−vis spectrometer (Avantes, 2.4 nm resolution) equipped with a 2024 pixel CCD detector array. Typical integration time for one spectrum was 100 ms.

For measurements the cell was mounted on an attachment for ATR measurements within the sample compartment of a Bruker Equinox-55 FTIR spectrometer equipped with a narrow-band MCT detector. Spectra were recorded at 4 cm^{-1}. The nanoparticle solution was passed through the cell and over the TiO_2 film at a flow rate of 0.2 mL min^{-1} by means of a peristaltic pump (Ismatec, Reglo 100). Some experiments were performed in the absence of oxygen. For this nitrogen was bubbled through the water. Irradiation of the sample with UV light was carried out using a 75 W Xe arc lamp. The UV light from the source was guided to the cell via two fiber bundles. The light was passed through a 5 cm water filter to remove any infrared radiation. Schott UG 11 and BG 42 (50 × 50 × 1 mm) broadband filters from ITOS were used to remove visible light (transmission below 380 nm). To check the influence of the visible light, some experiments were performed with a GG 420 filter (ITOS) instead that blocks the light below 400 nm. An estimate based on the supplier specifications gave an irradiance at the sample of slightly less than 2 mW cm^{-2}. For this estimate we considered the specified spectral irradiance of the arc lamp, the optical throughput of the lamp housing (rear window, beam condenser), the throughput through the fiber bundle, the transmittance of the optical filters, the reflection loss at the liquid filter and the cell window and the irradiated area (see Supporting Information for quantitative data). All experiments were performed at room temperature.

The adsorption of gold nanoparticles on the TiO_2 film was studied simultaneously by ATR-IR and UV−vis spectroscopy in the following way. After preparation of the TiO_2 film (70 μm) the cell for simultaneous ATR-IR and UV−vis measurements was assembled and mounted within the compartment of

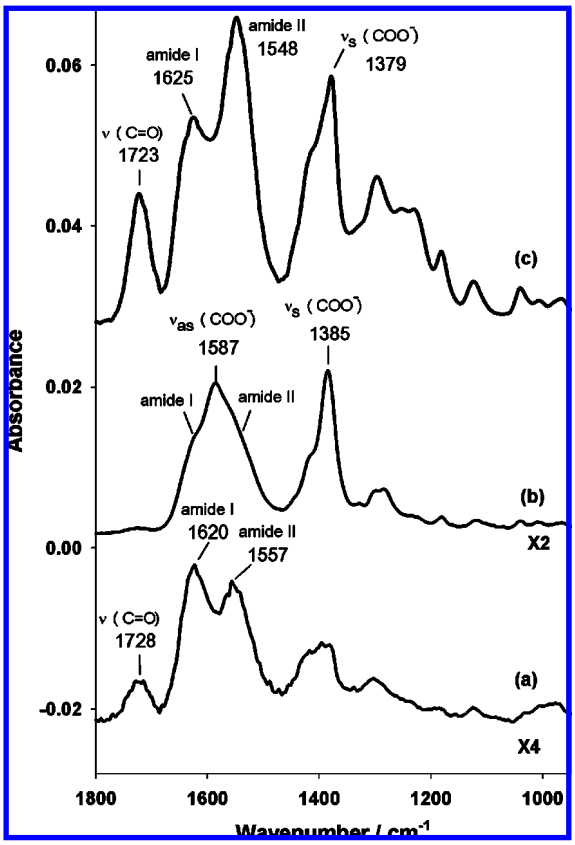

Figure 1. ATR-IR spectra of NAC-protected gold nanoparticles at pH 3 (c) and pH 5.5 (b) adsorbed on a TiO_2 film (4 μm). For comparison a spectrum of NAC adsorbed on TiO_2 at pH 3 is also shown (a). The spectra were recorded 1 h after starting adsorption from nanoparticle solution (1 mg in 1 mL). As the reference for the calculation of the absorbance spectra served the TiO_2 film before adsorption in the presence of water at the corresponding pH.

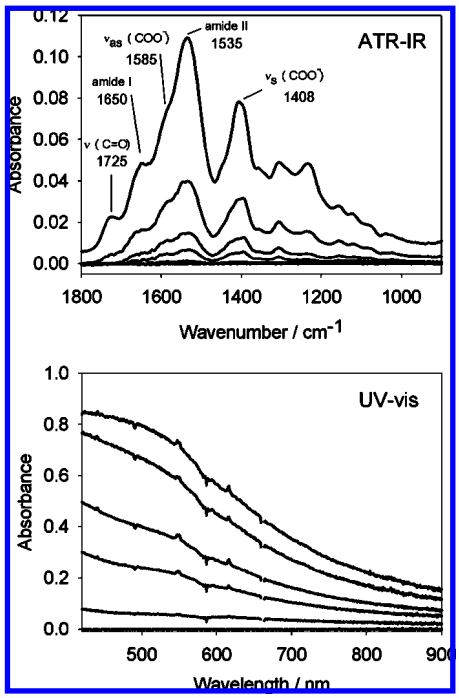

Figure 2. ATR-IR and UV−vis spectra recorded while flowing a solution (8 mg in 30 mL water) of GSH-protected gold nanoparticles over a TiO_2 film (70 μm) at pH 3. The TiO_2 film before adsorption in the presence of water at pH 3 served as the reference condition for calculation of the absorbance spectra. Spectra were recorded 0, 12, 19, 27, 47 and 89 min after starting the flow of nanoparticles.

the FTIR spectrometer. Then water at pH 3 was flowed through the cell until the ATR-IR spectra were stable (about 1 h). After that, the flow was switched (at time $T = 0$) to the nanoparticle solution (GSH-protected gold nanoparticles, 8 mg in 30 mL) and ATR-IR as well as UV−vis spectra were recorded simultaneously. Between the UV−vis measurements a shutter prevented extensive exposure of the catalyst to UV light.

Samples for transmission electron microscopy (TEM) were collected by scratching the TiO_2 film off the internal reflection element after the experiment. TEM images were recorded with a Philips C200 electron microscope operated at 200 kV. The sample was dispersed in water and a drop was cast onto a carbon-coated copper grid.

Results and Discussion

Adsorption of Monolayer-Protected Gold Nanoparticles on TiO_2. Figure 1 shows ATR-IR spectra that were recorded while flowing solutions of NAC-protected gold nanoparticles at pH 3 (spectrum c) and 5.5 (spectrum b) over a ca. 4 μm thick TiO_2 film on a Ge internal reflection element. The spectra were recorded 30 min after starting the flow of nanoparticle solution. Clear signals are observed in the ATR-IR spectra, which can be assigned to NAC adsorbed on the nanoparticles. It should be noted that the solutions do not contain detectable amounts of free NAC, as was verified by ^{1}H NMR spectroscopy. The almost complete absence of a band above 1700 cm^{-1} in Figure 1b indicates that at pH 5.5 the carboxylic acid group of NAC adsorbed on the gold particles is deprotonated. The pK_a value of NAC is 3.2.[26] The most significant bands at 1587 and 1385 cm^{-1} can be assigned to ν_{as}(COO−) and ν_s(COO−) vibrational modes, respectively, of the deprotonated carboxylic acid group.[27] The shoulders on the former band can be assigned to amide I and amide II modes. At pH 3 (Figure 1c) a significantly different spectrum was observed. Most evident is the appearance of a band at 1723 cm^{-1}, which shows that part of the acid groups are now protonated. At the same time the carboxylate band at 1379 cm^{-1} confirms the presence of deprotonated acid groups. Hence, at pH 3 both ionic forms coexist.

Figure 1 also reveals that at pH 3 the amount of adsorbed nanoparticles is considerably larger than at pH 5.5. Because the spectrum changes qualitatively with pH a relative quantification of the adsorbed amount of nanoparticles at the two pH values is difficult. Judging by the weak bands between 1000 and 1200 cm^{-1}, which do not shift with pH, and which hardly change intensity upon changing pH in solution, about 6 times more nanoparticles are adsorbed at pH 3 than at pH 5.5. When water at the corresponding pH flows over the sample, the nanoparticles slowly desorb from the surface at pH 5.5, whereas almost no desorption is observed at pH 3 (see also later). This behavior indicates that the adsorption and binding to the surface is charge-driven. At both pH values the NAC covered gold nanoparticles are negatively charged, the average charge per particle being larger at pH 5.5, as evidenced by the ATR-IR spectra given in Figure 1. However, pH 5.5 is closer to the isoelectric point (IEP) of P25, which is in the range 6.4−7.0.[28,29] Therefore, the TiO_2 surface is far less charged at this pH, whereas at pH 3 it is strongly positively charged, which explains the stronger adsorption at the latter pH.

Figure 1a also shows an ATR-IR spectrum of NAC (i.e., in the absence of nanoparticles) adsorbed on TiO_2 at pH 3. Significant differences between the spectra of adsorbed NAC and NAC-protected gold nanoparticles are observed. First of

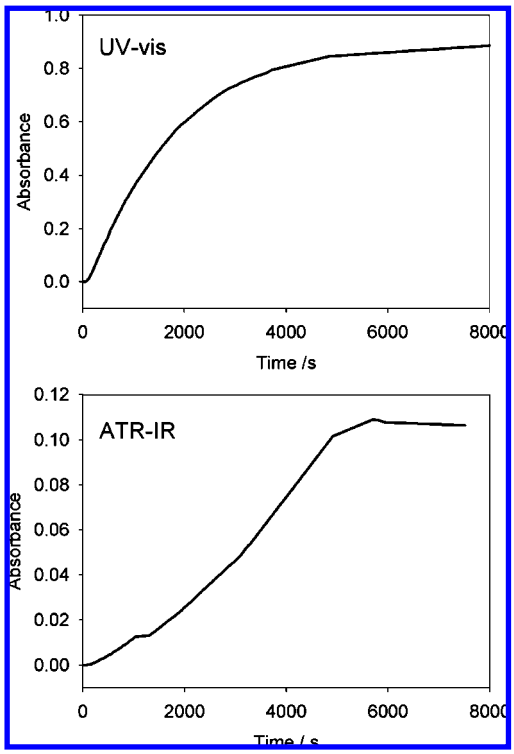

Figure 3. ATR-IR signal at 1536 cm^{-1} and UV−vis signal at 550 nm as a function of time that were recorded while flowing a solution (8 mg in 30 mL water) of GSH-protected gold nanoparticles over a TiO_2 film (70 μm) at pH 3 (see experiment shown in Figure 2). Note that in between UV−vis measurements the sample was in the dark.

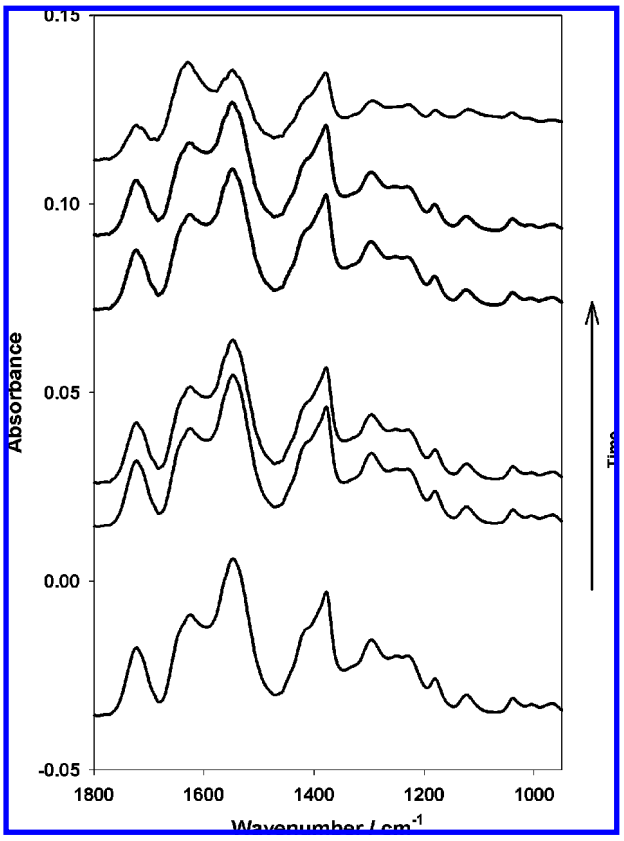

Figure 4. ATR-IR spectra of NAC-protected gold nanoparticles adsorbed on a TiO_2 film (4 μm). The bottom spectrum was recorded at the end of adsorption. The following two spectra were recorded during flowing water in the dark and the three top spectra during UV illumination. Water at pH 3 was flowed over the sample during illumination. Before illumination the nanoparticles were adsorbed at pH 3 for 2 h. The last spectrum (top) was recorded 95 min after starting the illumination.

all, the absolute intensity of the signals is about 1 order of magnitude larger for the particles. However, the spectra are also qualitatively different. Slight band shifts are observed in addition to important changes in relative intensity. For example, the relative strength of the two intense bands at 1620 and 1557 cm^{-1} associated with amide I and amide II vibrations changes strongly. The intensity of the band at 1728 cm^{-1} furthermore indicates that the degree of deprotonation of NAC on TiO_2 is larger than the one for NAC on the gold particles at the same pH. Carboxylates have a strong affinity to TiO_2.[30] For NAC adsorbed on gold it was shown that the carboxylate interacts with the gold surface in addition to the thiol.[27] Vibrational circular dichroism (VCD) moreover indicated that this is also the case for the gold nanoparticles investigated here.[21] The qualitative differences in the NAC spectra may point toward a different conformation of the molecule in the two situations. When the NAC-protected gold nanoparticles are adsorbed, some NAC molecules are in direct contact with the TiO_2 surface. Whether these molecules interact via the carboxylate with the TiO_2 cannot be answered on the basis of the spectra.

Figure 2 shows a series of ATR-IR and UV−vis spectra that were recorded in situ while flowing a solution of L-glutathione (γ-glu-cys-gly, GSH)-protected nanoparticles over a TiO_2 film (ca. 70 μm) at pH 3. At this pH GSH in solution is partially negatively charged,[31] similar to NAC. Furthermore, it has been shown that the adsorption of GSH on gold favors deprotonation of the carboxylic acid group at the gly part of the molecule.[32] The most significant bands in the spectrum can be assigned to the C═O stretching mode of protonated acid groups (COOH) at 1725 cm^{-1}, to the amide I and amide II modes at 1650 and 1535 cm^{-1}, and to the antisymmetric and symmetric carboxylate vibrations at 1585 (shoulder) and 1408 cm^{-1}. In agreement with the ATR-IR spectra the UV−vis spectra indicate the adsorption of the nanoparticles on the TiO_2 film. There is no sign of a plasmon band in the UV−vis spectra, which confirms that the particle diameter is equal to or smaller than 2 nm,[33] in agreement with transmission electron microscopy. The optical absorption spectrum of such small particles is characterized by a strongly increasing signal toward shorter wavelengths.

For experiments performed with a thin film (Figure 1, about 4 μm), the adsorption process was finished within a few minutes, considering the increase of the ATR-IR signals with time. In contrast, significant retardation was observed for experiments performed with thicker films. Figure 3 shows the ATR-IR signal at 1550 cm^{-1} and the UV−vis signal at 450 nm as a function of time for an experiment where GSH-protected gold nanoparticles were adsorbed on a thick TiO_2 film (70 μm). The two signals were recorded simultaneously and in situ. Obviously, the shape of the two curves is significantly different, which is due to the different sampling geometry for the two techniques. In the UV−vis experiment the sample is probed perpendicular to the film and therefore an average over the whole film between the IRE/film interface and the film/solution interface is obtained. In contrast, ATR-IR only probes the volume the closest to the IRE. An estimate of the penetration depth d_p at 1500 cm^{-1} [19] based on the effective refractive index of the wet TiO_2 film yields a value of 0.52 μm. To estimate the effective refractive index of the film, the refractive index of water (1.33) and anatase (2.49) and a void fraction of 0.5 were assumed.[34] Figure 3 shows that it takes about 2 h until the signals are stable. The combined information obtained from the two techniques reveals that mass transport through the thick film (70 μm) plays an important role.

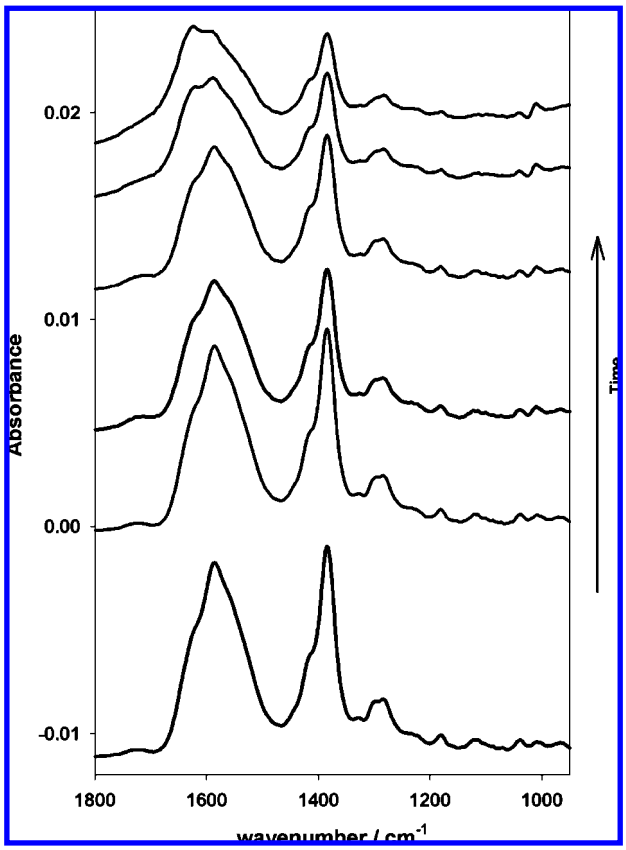

Figure 5. ATR-IR spectra of NAC-protected gold nanoparticles adsorbed on a TiO_2 film (4 μm). The bottom spectrum was recorded at the end of adsorption. The following two spectra were recorded during flowing water in the dark and the three top spectra during UV illumination. Water at pH 5.5 was flowed over the sample during illumination. Before illumination the nanoparticles were adsorbed at pH 5.5 for 2 h. The last spectrum (top) was recorded 95 min after starting the illumination.

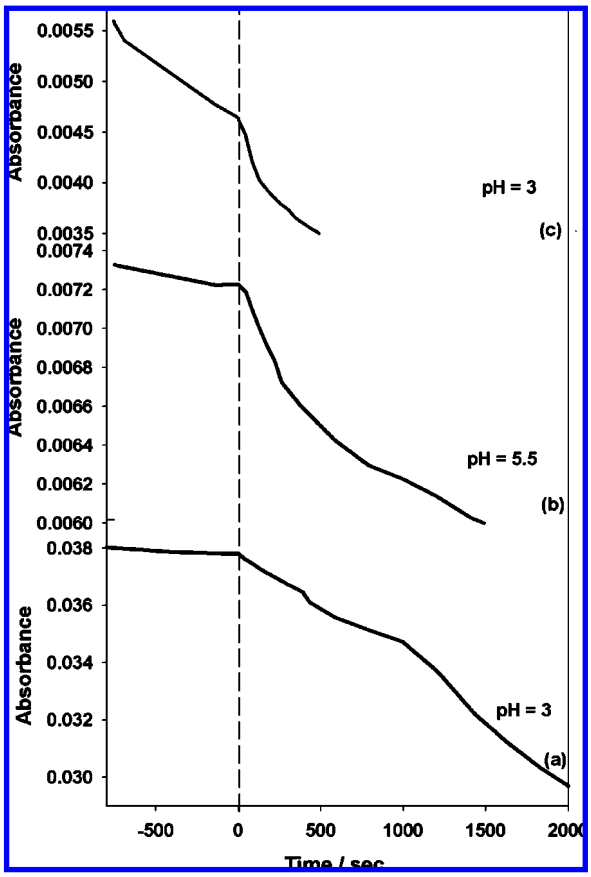

Figure 6. ATR-IR signals at 1546 (a) and 1585 cm^{-1} (b) as a function of time corresponding to the experiment described in Figures 4 and 5. The ATR-IR signal at 1552 cm^{-1} of NAC adsorbed on TiO_2 at pH 3 as a function of time is also shown for comparison (c).

This leads to a gradient of adsorbed particles perpendicular to the IRE surface within the film. For example, after 2000 s more than 60% of a full coverage is achieved on average over the whole film (see UV−vis), whereas on the part the closest to the IRE only about 20% of a full coverage is achieved (see ATR-IR). Adsorption on the outer part of the film is therefore fast, similar to what was observed for the thin film by ATR-IR, whereas adsorption on the inner part of the film is limited by intrafilm mass transport of the nanoparticles. In this context it is important to note that, upon formation of the film, agglomeration of the TiO_2 particles leads to a porous network with pores of about 10 nm, as can be judged from inspection of TEM images of the dried powder (see Supporting Information). The size of the pores is therefore only a few times larger than the size of the nanoparticles itself (gold core plus protection layer). The mass transport within the TiO_2 film is likely quite complex. The diffusion of the particles through the porous film depends on the charge of both partners (particle and film), besides other factors like porosity of the film. However, upon adsorption of the particles on the outer surface of the film, the surface charge changes locally, which changes the effective diffusion constant. In fact the latter becomes dependent on time and space within the film.

Illumination of the Adsorbed Gold Nanoparticles. Figures 4 and 5 show two series of ATR-IR spectra recorded while flowing water over the sample during UV illumination at pH 3 (Figure 4) and pH 5.5 (Figure 5). Before these experiments, a solution of NAC-protected gold nanoparticles was flowed over the TiO_2 film for 25 min followed by a flow of water for 45 min. Clearly the signals associated with NAC adsorbed on the gold nanoparticles decrease with time upon illumination.

Figure 6 shows the ATR-IR signals at 1546 (a) and 1585 cm^{-1} (b) as a function of time corresponding to the experiments shown in Figures 4 and 5. The dashed vertical line indicates the start of the illumination. Clearly, at pH 5.5 some desorption of NAC-protected nanoparticles is observed in the dark, whereas at pH 3 desorption during water flow is insignificant. Upon illumination the NAC bands decrease. Interestingly, at pH 3 the decrease of the signal is relatively slow during the first 1000 s of illumination, but after that initial period the rate increases.

Figure 6 also shows the signal at 1552 cm^{-1} of NAC adsorbed on TiO_2 at pH 3 as a function of time (trace c). In this experiment NAC was adsorbed first before flowing water over the sample. Obviously, in the dark NAC desorbs from the TiO_2 surface at much higher rate than the NAC-protected gold nanoparticles (compare with Figure 6a). The stronger adsorption of the nanoparticles compared to NAC could be due to the stronger electrostatic and van der Waals interaction or due to multiple interactions between particle and TiO_2 via carboxylate groups.

When the UV-light is turned on, NAC is removed fast. The relative decrease for NAC is larger than the one for the NAC-protected gold nanoparticles, even when taking into account desorption in the dark. In the case of NAC the signals decrease by about 15% within 500 s, whereas for the NAC-protected gold particles a decrease of only 6.6% is observed under the same conditions. The different relative rates point toward different light-induced processes in the two situations. This is

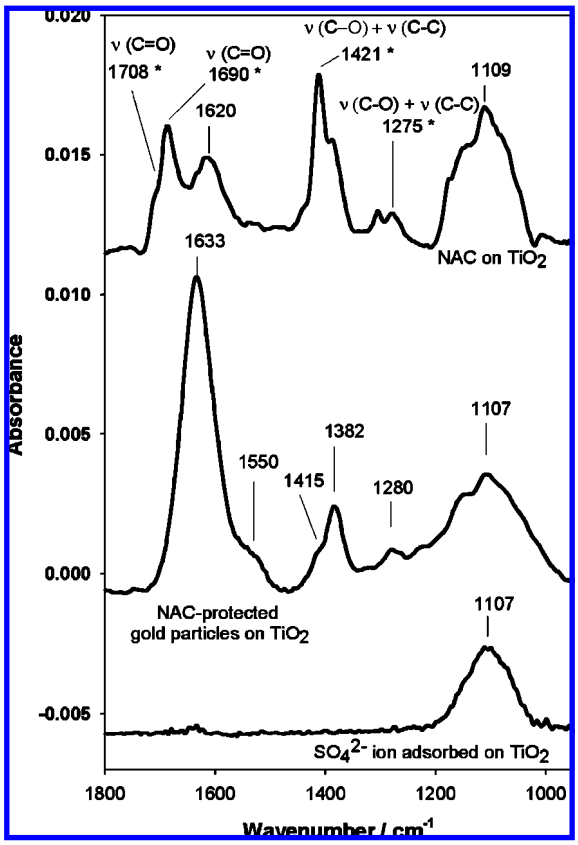

Figure 7. ATR-IR difference spectra corresponding to illumination experiments of the NAC-protected gold particles on TiO_2 (middle spectrum) and of NAC on TiO_2 (top spectrum) at pH 3. The difference spectra correspond to the last spectrum recorded during illumination from which the spectrum recorded before starting illumination was subtracted, in such a way that the NAC signals vanish. The spectra thus highlight the species that are formed upon illumination. Bands labeled with an asterisk are associated with oxalate species. The bottom spectrum was obtained after flowing a solution of H_2SO_4 (1 mM) over a calcined Au/TiO_2 catalyst.

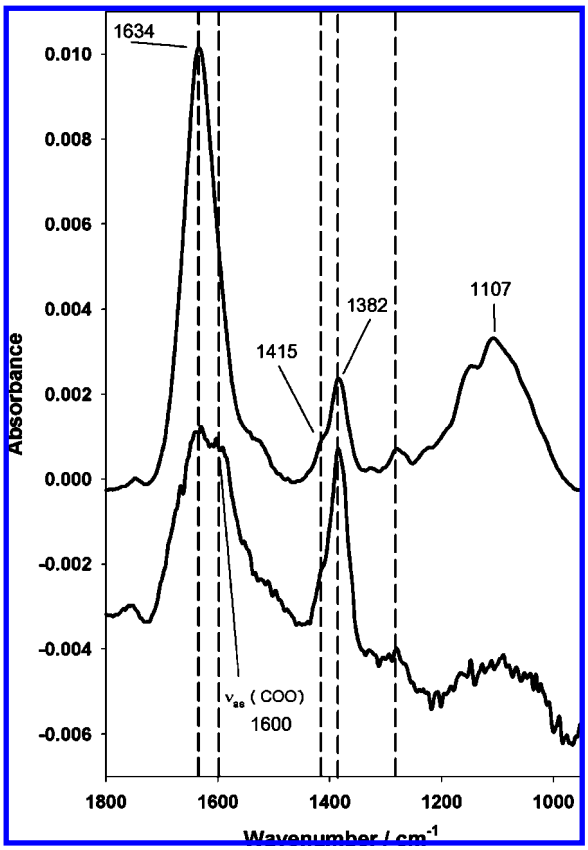

Figure 8. ATR-IR difference spectra corresponding to an experiment where NAC-protected gold particles on TiO_2 were illuminated at pH 3. The bottom spectrum corresponds to a difference spectrum recorded during the first 1000 s of illumination (see Figure 6). The top spectrum was recorded at the end of illumination.

confirmed by Figure 7 (top and middle), showing difference spectra recorded during irradiation of NAC and NAC-protected gold nanoparticles, respectively, on TiO_2. These spectra reveal the species formed during irradiation. Obviously the two spectra in Figure 7 are rather different. The middle spectrum (NAC-protected gold nanoparticles) is dominated by a band at 1633 cm^{-1}. Part of this band may originate from incompensation of water. When NAC or NAC-protected gold nanoparticles leave the TiO_2 surface, the amount of water probed by the evanescent field increases, which results in a water signal in the difference spectrum. The broad band centered around 1100 cm^{-1} can be assigned to oxidized sulfur species such as sulfate. Indeed, adsorption of sulfate on Au/TiO_2 resulted in a similar broad signal at 1100 cm^{-1}, as can be seen in Figure 7, bottom. It should be noted that this band did not appear in experiments where the sample was irradiated by visible light only (see Supporting Information). In the absence of oxygen this band was also missing (see Supporting Information). The origin of the other bands observed at 1280, 1382, (shoulder at 1415 cm^{-1}) and about 1550 cm^{-1} is less clear. The latter band could be due to amide and/or carboxylate vibrations. Upon illumination of NAC on TiO_2 (top spectrum in Figure 7), the broad sulfate signal at 1100 cm^{-1} is also observed. The most important differences with respect to the corresponding spectrum of NAC-protected gold nanoparticles (Figure 7 middle) are the characteristic signals associated with oxalate species ($^-OOC-COO^-$) at 1690 (with a shoulder at 1708 cm^{-1}), 1421, and 1275 cm^{-1}.[30] In addition, the band at 1620 cm^{-1} can be assigned to a carboxylate vibration of a newly formed species. Oxalate species on TiO_2 have been observed previously, for example, during photocatalytic mineralization of malonic and succinic acid[25,35] and the photoassisted reaction of glyoxylic acid on TiO_2.[36] Oxalate seems to be a ubiquitous species during irradiation of TiO_2 in the presence of carboxylic acids, and its observation on the TiO_2 surface upon irradiation of adsorbed NAC is therefore not too surprising. On the other hand, there is no sign of oxalate in the corresponding spectrum for the NAC-stabilized gold nanoparticles. This shows different reaction pathways for NAC in the two cases.

It is known that the photoexcited electron can be transferred from TiO_2 to adsorbed metal particles.[37] Alternatively, it has been shown that photoexcitation of gold particles can lead to an inverse flow of electrons, i.e., from the gold particle to the TiO_2.[6] In contrast to the bulk metal, gold nanoparticles have been shown to be photoluminescent. Small gold nanoparticles show increased photochemical activity because of their high surface to volume ratio and their particular electronic properties.[38] The thiolate on the gold may thus act as an electron donor to the gold particle and therefore be oxidized. Upon irradiation, the observed oxidized sulfur species could directly be formed on the gold particles similarly to what is noticed for thiols adsorbed on gold surfaces upon UV exposure.[16] Our experiments show that the UV part of the light is responsible for the deep oxidation of the sulfur in the presence of dissolved oxygen, although the gold particles can be excited by visible light as well. On the other hand, the same species are also apparent on

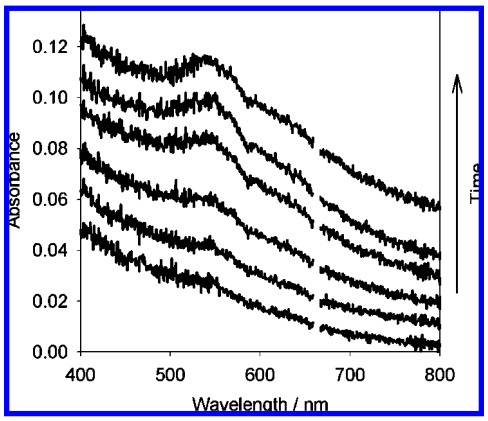

Figure 9. UV−vis spectra recorded while illuminating GSH-protected gold nanoparticles adsorbed on a TiO_2 film. The spectra were recorded (from bottom to top) 30, 40, 60, 90, 120 and 150 min after starting the illumination. During illumination water at pH 3 was flowed over the sample. The spectra are offset for clarity. Note that the UV−vis source of the spectrometer was used to illuminate the sample and that in between measurements the sample was illuminated.

the TiO_2 surface upon irradiation of NAC in the absence of the gold particles, which is ascribed to the action of the TiO_2 photocatalyst. The observation of sulfate species in both cases tempts one to assign their formation to the same process, i.e., the action of the TiO_2 photocatalyst. However, we think that this is not the case because this would imply desorption of the thiol from the gold particle prior to reaction on the TiO_2, which is rather unlikely. Possibly, the oxidation of the thiols directly takes place on the gold particles, similar to what was reported for the oxidation of self-assembled monolayers on gold surfaces.[16] The desorption of these compounds leads to partly naked gold particles.

Figure 8 shows difference spectra recorded at the beginning and at the end of illumination highlighting the species that are formed. The spectra are clearly different at the beginning of irradiation with relative strong bands at 1415 and 1382 cm^{-1} and relatively weak sulfate bands (1100 cm^{-1}). This indicates that the first bands are associated with less oxidized species, which are subsequently further oxidized to sulfates. Furthermore, a band at around 1600 cm^{-1} is observed at the beginning of irradiation that is possibly associated with a carboxylate group of a newly formed species. We propose that the oxidation of the sulfur is proceeding via different pathways in the two cases, i.e., directly on the gold particles in the case of the NAC-protected gold particles, similar to what was found for self-assembled monolayers of thiols on gold, and on the TiO_2 via photo-oxidation in the case of NAC. The absence of oxalate signals in the experiments conducted with the NAC-protected gold nanoparticles indicates that the formation of the oxalate is a process that takes place on the TiO_2 surface and not in solution and/or on the gold particles. Upon illumination of TiO_2 radicals (hydroxyl, $O_2^{-\cdot}$) are formed, which can react with dissolved species or species adsorbed on the gold nanoparticles. The absence of oxalate in the case of NAC-protected gold nanoparticles indicates that the formation of oxalate is not directly mediated by such radicals. It should be noted that, when NAC is adsorbed onto a gold−TiO_2 catalyst, oxalate is observed under irradiation.

Effect of Illumination on Gold Particle Size. When the gold nanoparticles adsorbed on the TiO_2 film were illuminated, a color change was observed. Before UV exposure the film was brownish, whereas after exposure its appearance was violet, which indicates a change in the metal core of the particles. Note

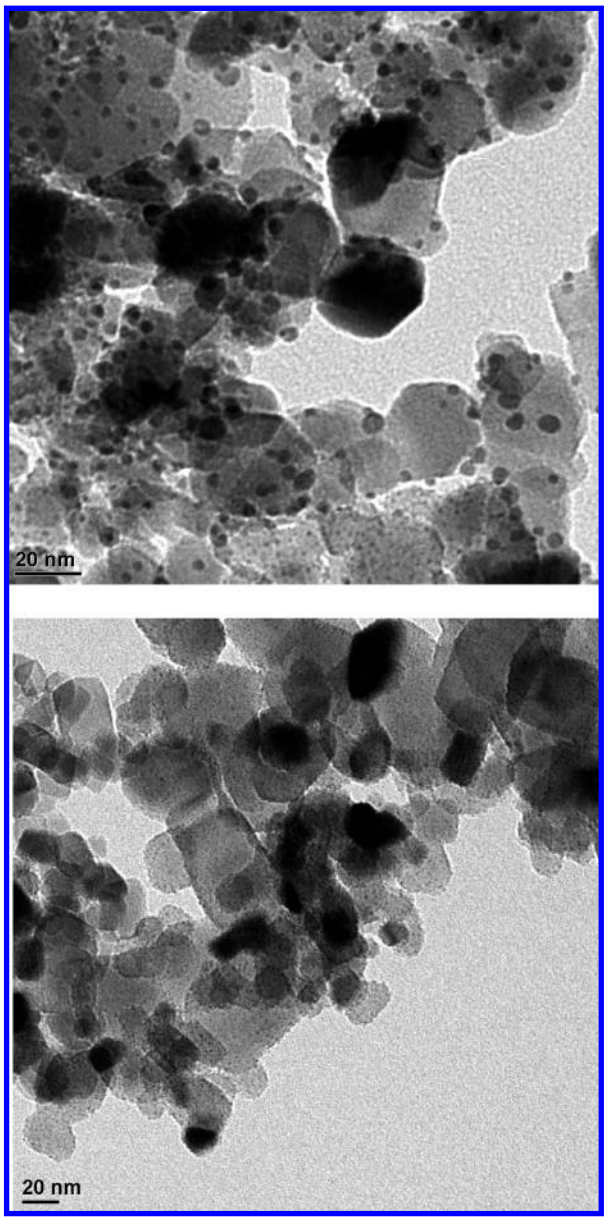

Figure 10. Transmission electron microscopy (TEM) images of NAC-protected gold nanoparticles on TiO_2 before (bottom) and after (top) 100 min of UV illumination.

that this color change was not observed when the sample was exposed to visible light only or to UV light in the absence of oxygen. Indeed, in situ UV−vis spectroscopy revealed the development of a surface plasmon band at around 540 nm with time upon exposure to UV light in the presence of oxygen (see Figure 9), which indicates the presence of gold particles larger than about 3 nm. This was confirmed by transmission electron microscopy (TEM) of the unexposed and exposed sample as shown in Figure 10.

The TEM of the sample after adsorption of NAC-protected gold nanoparticles reveals well-dispersed and very small gold nanoparticles on the TiO_2. The particles are on the order of 1 nm in diameter and distributed evenly over the whole surface. After UV illumination the particles are considerably larger (5 nm).

The increase of the mean particle size upon illumination shows that the NAC-protected gold nanoparticles are mobile on the TiO_2 surface at room temperature under our conditions. The increase in particle size has to do with the (partial) removal of the NAC protection layer by the UV exposure, thus enabling

SCHEME 2: Pictorial View of the Processes Occurring upon Illumination of Passivated Gold Particles Adsorbed on TiO_2

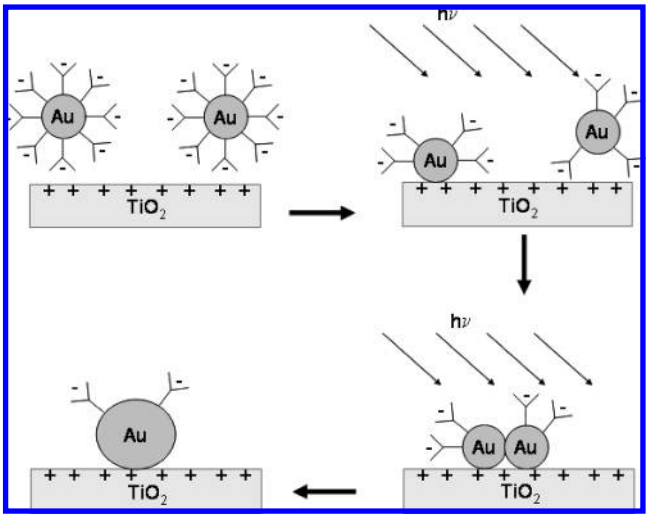

contact between gold cores. Note that with an intact NAC protection layer the gold nanoparticles can be dried and redispersed without sintering. The particles in the TEM images do not seem to be agglomerates of individual smaller particles. This indicates that the smaller particles melt together to form larger particles at room temperature (Scheme 2). Both the removal of the protection layer and the mobility of the particles on the support likely depend on the nature of the passivating molecules. The latter should be considered as an important parameter for the tailoring of supported gold catalysts prepared by the method applied here. Interestingly, in a recent report it was proposed, on the basis of transmission electron microscopy, that gold nanoparticles linked to the TiO_2 through 3-mercaptopropionic acid (MPA) were immobile under UV irradiation.[5] Furthermore, it was proposed that the MPA withstands the photoreactions, although no direct molecular level information was provided. The apparently different behavior of MPA- and NAC-protected gold nanoparticles on TiO_2 may be due to the different chemical nature of the passivating molecule and the different conditions for the preparation of the material.

The different species observed at the very beginning of irradiation of NAC-protected gold nanoparticles and at the end (Figure 8) may be related to the finding that at the beginning the rate of disappearance of the NAC signals is slow and accelerates afterward (see Figure 6a). One may speculate that this change has to do with the reaction of the NAC molecules on the gold particles that are in direct contact with the TiO_2 surface. Once these are consumed, the better contact between gold and TiO_2 leads to a higher electron-transfer rate, which furthermore accelerates NAC decomposition. Alternatively, it has been shown recently that the rate of charge transfer between TiO_2 and gold particle increases with the size of the latter.[39] Therefore, in our case the charge transfer should be initially slow for the small particles. Once the particle size has increased, the electron-transfer rate increases as well, thus accelerating NAC decomposition.

Conclusions

The combination of attenuated total reflection infrared (ATR-IR) and UV−vis spectroscopy allows one to study mass transport within porous films supported on internal reflection elements due to the different sampling geometry of the two techniques. This combination revealed that the adsorption of gold nanoparticles covered by thiols onto porous films of TiO_2 is significantly limited by mass transport within the film. Upon illumination the adsorbed thiolates on the gold nanoparticles are partly removed and oxidized sulfur species such as sulfates are observed on the surface. The latter species are also observed when *N*-acetyl-L-cysteine directly adsorbed on TiO_2 is illuminated, i.e., in the absence of gold particles. However, the mechanism of *N*-acetyl-L-cysteine decomposition seems to be different in the two cases, because in the latter situation a large amount of oxalate is observed on the TiO_2 surface, which is not the case for the gold nanoparticles. The partial removal of the thiolate protection layer leads to agglomeration of small particles and the formation of larger ones, which can be followed in situ through UV−vis spectroscopy by the development of a surface plasmon resonance band. This is also confirmed by TEM measurements. This finding shows that the protected particles are mobile on the TiO_2 surface at room temperature and in water, despite the presence of multiple carboxylate groups. For the synthesis of tailored catalysts it might be advantageous to prepare materials with even smaller gold particles than the ones obtained in this work. This requires the reduction of particle mobility during removal of the thiolate layer for example by using other thiols or by lowering the temperature during illumination.

Acknowledgment. Financial support by the Swiss National Science Foundation is kindly acknowledged. We thank the ComLab (CSEM and University of Neuchâtel) for providing TEM facilities.

Supporting Information Available: ATR-IR spectrum for experiment with visible light and for experiment with UV light in the absence of oxygen. TEM image of agglomerated TiO_2 particles. Estimation of the irradiance at the sample. This information is available free of charge via the Internet at http://pubs.acs.org.

References and Notes

(1) Sun, S. Q.; Mendes, P.; Critchley, K.; Diegoli, S.; Hanwell, M.; Evans, S. D.; Leggett, G. J.; Preece, J. A.; Richardson, T. H. *Nano Lett.* **2006**, *6*, 345.
(2) Haruta, M.; Kobayashi, T.; Sano, H.; Yamada, N. *Chem. Lett.* **1987**, 405.
(3) Haruta, M.; Yamada, N.; Kobayashi, T.; Iijima, S. *J. Catal.* **1989**, *115*, 301.
(4) Chou, J.; McFarland, E. W. *Chem. Commun.* **2004**, 1648.
(5) Li, J.; Zeng, H. C. *Chem. Mater.* **2006**, *18*, 4270.
(6) Tian, Y.; Tatsuma, T. *J. Am. Chem. Soc.* **2005**, *127*, 7632.
(7) Kamat, P. V. *J. Phys. Chem. C* **2007**, *111*, 2834.
(8) Valden, M.; Lai, X.; Goodman, D. W. *Science* **1998**, *281*, 1647.
(9) Stiles, A. B.; Koch, T. A. *Catalyst Manufacture*, 2nd ed.; Dekker: New York, 1995.
(10) Schmid, G. *Chem. Rev.* **1992**, *92*, 1709.
(11) Brust, M.; Walker, M.; Bethell, D.; Schiffrin, D. J.; Whyman, R. *J. Chem. Soc., Chem. Commun.* **1994**, 801.
(12) Tada, H.; Soejima, T.; Ito, S.; Kobayashi, H. *J. Am. Chem. Soc.* **2004**, *126*, 15952.
(13) Dasog, M.; Scott, R. W. J. *Langmuir* **2007**, *23*, 3381.
(14) Sandhyarani, N.; Pradeep, T. *Chem. Phys. Lett.* **2001**, *338*, 33.
(15) Kell, A. J.; Alizadeh, A.; Yang, L.; Workentin, M. S. *Langmuir* **2005**, *21*, 9741.
(16) Brewer, N. J.; Rawsterne, R. E.; Kothari, S.; Leggett, G. J. *J. Am. Chem. Soc.* **2001**, *123*, 4089.
(17) Tian, Y.; Notsu, H.; Tatsuma, T. *Photochem. Photobiol. Sci.* **2005**, *4*, 598.
(18) Linsebigler, A. L.; Lu, G.; Yates, J. T. *Chem. Rev.* **1995**, *95*, 735.
(19) Harrick, N. J. *Internal reflection spectroscopy*; Interscience Publishers: New York 1967.
(20) Bürgi, T.; Baiker, A. *Adv. Catal.* **2006**, *50*, 228.
(21) Gautier, C.; Bürgi, T. *Chem. Commun.* **2005**, 5393.
(22) Gautier, C.; Bürgi, T. *J. Am. Chem. Soc.* **2006**, *128*, 11079.

(23) Danion, A.; Disdier, J.; Guillard, C.; Abdelmalek, F.; Jaffrezic-Renault, N. *Int. J. Appl. Electromagn. Mechanics* **2006**, *23*, 187.
(24) Bürgi, T. *J. Catal.* **2005**, *229*, 55.
(25) Dolamic, I.; Bürgi, T. *J. Phys. Chem. B* **2006**, *110*, 14898.
(26) Juch, R.; Birrenbach, G.; Pflugshaupt, C. United States Patents, 1995.
(27) Bieri, M.; Bürgi, T. *J. Phys. Chem. B* **2005**, *109*, 22476.
(28) Dionysiou, D. D.; Suidan, M. T.; Bekou, E.; Baudin, I.; Laine, J. M. *Appl. Catal. B-Environ.* **2000**, *26*, 153.
(29) Gumy, D.; Morais, C.; Bowen, P.; Pulgarin, C.; Giraldo, S.; Hajdu, R.; Kiwi, J. *Appl. Catal. B-Environ.* **2006**, *63*, 76.
(30) Hug, S.; Bahnemann, D. *J. Electron. Spectrosc. Relat. Phenom.* **2006**, *150*, 208.
(31) Rabenstein, D. L. *J. Am. Chem. Soc.* **1973**, *95*, 2797.
(32) Bieri, M.; Bürgi, T. *Langmuir* **2005**, *21*, 1354.
(33) Alvarez, M. M.; Khoury, J. T.; Schaaff, T. G.; Shafigullin, M. N.; Vezmar, I.; Whetten, R. L. *J. Phys. Chem. B* **1997**, *101*, 3706.
(34) Braun, M. M.; Pilon, L. *Thin Solid Films* **2006**, *496*, 505.
(35) Dolamic, I.; Bürgi, T. *J. Catal.* **2007**, *248*, 268.
(36) Ekström, G. N.; McQuillan, A. J. *J. Phys. Chem. B* **1999**, *103*, 10562.
(37) Subramanian, V.; Wolf, E. E.; Kamat, P. V. *J. Am. Chem. Soc.* **2004**, *126*, 4943.
(38) Schmid, G. *Nanoparticles: From Theory to Applications*; Wiley-VCH Verlag GmbH: Weinheim, 2004.
(39) Kim, J.; Lee, D. *J. Am. Chem. Soc.* **2007**, *129*, 7706.